International Journal of Rock Mechanics & Mining Sciences 150 (2022) 104980

Contents lists available at ScienceDirect

International Journal of Rock Mechanics and Mining Sciences

journal homepage: www.elsevier.com/locate/ijrmms

Drag bit/rock interface laws for the transition between two layers

Arviandy G. Aribowo [a,*], Roeland Wildemans [a], Emmanuel Detournay [b], Nathan van de Wouw [a,b]

[a] Department of Mechanical Engineering, Eindhoven University of Technology, Eindhoven, The Netherlands
[b] Department of Civil, Environmental, and Geo-Engineering, University of Minnesota, Minneapolis, USA

ARTICLE INFO

Keywords:
Drilling
Transitional phase
Cutting process
Frictional contact
Specific energy
Drilling strength
E–S diagram
Drilling efficiency

ABSTRACT

This paper extends bit/rock interface laws for drag (PDC) bits, originally formulated for homogeneous rocks, to the transition between two rock layers with distinct mechanical properties. It formulates a set of relations between the weight-on-bit, the torque-on-bit, the depth-of-cut per bit revolution, and the engagement parameter of the bit in the lower rock layer. This model enables us to extend the 2D $E-S$ diagram for the homogeneous case to a 3D $E-S$ diagram for the transitional case, where the third dimension is related to the engagement parameter. Moreover, this model is used to derive an expression for the drilling efficiency for the transitional phase. Examples are provided for describing the 3D $E-S$ diagram and drilling efficiency under the condition of quasi-stationary drilling (i.e., constant angular velocity, constant weight-on-bit). These examples show that the drilling efficiency depends nonlinearly on the bit engagement between the two rock layers. This intrinsic dependency is closely related to the bit shape.

1. Introduction

Exploration and production activities for the discovery and extraction of hydrocarbon and geothermal energy resources require to drill deep (even ultra-deep-water) well-bores into the targeted reservoir zones in the earth's crust where the resources are accumulated. Down-hole, self-excited vibrations are omnipresent phenomena when performing these drilling operations, which are typically done by rotary drilling systems equipped with Polycrystalline-Diamond-Compact (PDC) bits as sketched in Fig. 1(a). PDC bits (also known as a class-type of fixed cutter or drag bits) consist of several bit blades on which the PDC cutters are attached (see Fig. 1(b)).

The vibrations at the bit are primarily caused by the interaction between the bit and the rock formation.[2–4] In addition, the bit experiences transient vibrations when transitioning between two distinct layers[5–7]. Such drilling conditions can lead to fast changes in the weight-on-bit (WOB) and torque-on-bit (TOB) arising from the bit/rock interaction, and consequently affect the total dynamics of the drill–string system. These rapid load changes on the bit may lead to bit damage and drilling in interbedding formations may significantly affect drilling efficiency.[8–11] These observations motivate the development of a bit/rock interaction model for PDC bits transitioning between two layers.

The interface laws, originally introduced in Refs. 12–14 to describe the interaction between the rock and bit, have been used to analyze the response of drilling systems with PDC bits in *homogeneous* formations. In Refs. 15–19, these interface laws are utilized in the modeling and dynamic analyses of drill–string systems to explain the root-cause of the vibrations for drilling scenarios with PDC bits in *homogeneous* rock formations. The interface laws, being parameterized by the rock mechanical properties and the bit-design properties, couple the axial and torsional dynamics of the drill–string through both the regenerative effect (well-known in the scope of chatter phenomenon in the milling process[20]) and frictional contact. However, such interface laws for the case of the bit transitioning between two distinct rock layers are still missing in the literature.

The main contributions of this paper are as follows:

- Firstly, we extend the bit/rock interface laws for homogeneous formations to the transition between two layers (e.g., soft and hard layers of an interbedded formation as sketched in Fig. 1(a)). Specifically, we derive a set of relations between the dynamic variables (the WOB W, the TOB T) and the kinematic variable d for the depth-of-cut (DOC) produced per bit revolution and the evolution parameter U for the bit engagement in the associated lower layer during the transition. Parameter U represents how deep the bit has entered the lower layer.
- Secondly, by using this novel model, we extend the 2D $E-S$ diagram (with E being the mechanical-specific-energy (MSE) and S being the drilling strength) for the homogeneous case to 3D $E-S$ diagrams for the transitional case, where the third dimension is related to the engagement parameter U.

* Correspondence to: Department of Mechanical Engineering, Eindhoven University of Technology, PO Box 513, 5600 MB, Eindhoven, The Netherlands.
E-mail address: a.g.aribowo@tue.nl (A.G. Aribowo).

https://doi.org/10.1016/j.ijrmms.2021.104980
Received 26 June 2021; Received in revised form 8 November 2021; Accepted 13 November 2021

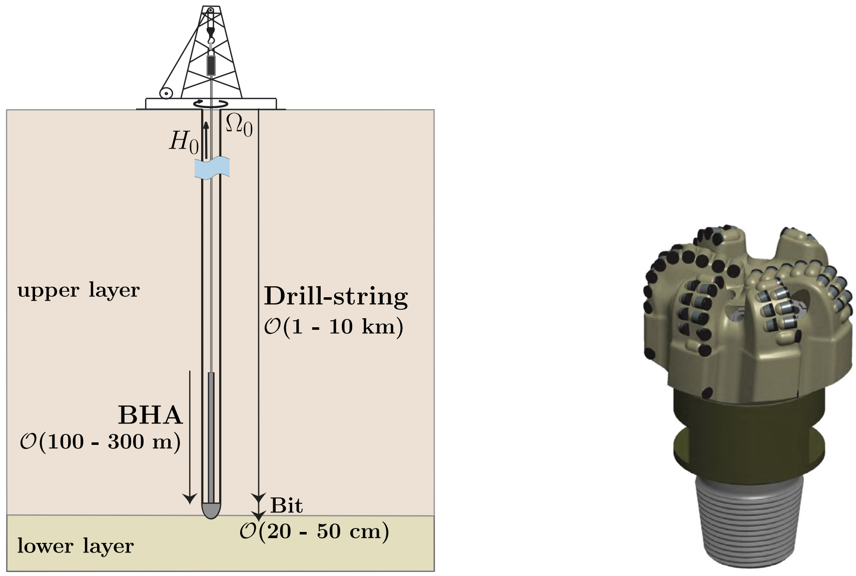

(a) Schematic overview. (b) PDC bit (after [1]).

Fig. 1. Rotary drilling system with PDC bit in drilling a vertical well-bore during a transitional phase between two rock layers.[1]

– Finally, this model is used to find an analytical expression for the drilling efficiency for the transitional case.

The paper is organized as follows. Section 2 summarizes the foundational formulation of the interface laws for the transitional phase, which consist of two components: *(i)* cutting and *(ii)* frictional contact. In Section 3, the dynamic variables in these components are explicitly formulated as function of the depth-of-cut and parameterized by the bit characteristics and the rock properties associated to the layer(s) with which the bit currently engages. Section 4 presents the extension of the $E-S$ diagram and of the drilling efficiency for the transitional phase. In Section 5, the MSE and the drilling efficiency are numerically investigated within a scenario of the transitional phase. Furthermore, the effect of the bit shape on the drilling efficiency is also explored. Finally, Section 6 draws conclusions.

2. Problem formulation

In this section, we formulate the foundations over which the interface laws are extended for the transitional phase between two rock layers. We recall some well-established concepts related to bit/rock interaction in *isotropic-homogeneous* rock formations. We also introduce some novel parameters related to the transitional phase that will be used in extending the interface laws.

2.1. Rate-independent interface laws and penetration per revolution of the bit

We consider the normal mode of bit/rock interaction, where the bit is drilling straight ahead. The response model of drilling with drag bits in this normal mode consists of a set of relations between the weight-on-bit W, the torque-on-bit T, the rate of penetration (ROP) V, and the angular velocity Ω.[13,14] In this work, we use the coordinate basis $(\mathbf{i}_x, \mathbf{i}_y, \mathbf{i}_z)$ of the PDC bit system (see Fig. 2(a)). The $\mathbf{i}_z$-axis coincides with the bit axis of symmetry while pointing ahead of the bit and the origin is selected at the reference point of the bit (located at the lowest point on the bit profile). The coordinate basis of the bit system can also be represented in the cylindrical coordinate basis $(\mathbf{i}_r, \mathbf{i}_\omega, \mathbf{i}_z)$ as depicted in Fig. 2(a).

The rate-independent bit/rock interface laws relate these dynamic variables (W, T) to the kinematic variable d. During the transitional phase between two rock layers, the extension of these interface laws are formulated to be parameterized by the bit engagement U in the lower layer (as the evolution parameter), such that

$$W = \widetilde{W}(d; U), \qquad T = \widetilde{T}(d; U). \tag{1}$$

These functions $\widetilde{W}, \widetilde{T}$ in (1) are averaged over at least one revolution of the bit. The relations are assumed to be rate-independent, as supported by experimental evidence from laboratory single cutter and drilling tests conducted under kinematic control.[21–24] The kinematic variable d can also be understood as the penetration per revolution of the bit, which represents the advance of the bit in the $\mathbf{i}_z$ direction; see Fig. 2(b). On the other hand, the parameter U determines the portion of the bit engaged in the lower layer during the transitional phase (to be detailed in Section 2.5). Herein, we assume *quasi-stationary* drilling conditions where the total WOB and the angular velocity (RPM) of the bit are constant.

2.2. Equivalent blade concept

The concept of *equivalent blade* introduced in Refs. 14, 25 is adopted to simplify the description of the interaction of the bit with the rock. To illustrate this concept, first we consider that all PDC cutters mounted along a bit blade on the bit body are as the outer (cutting) edge of the bit defined by a two-dimensional curve C (red line) illustrated in Fig. 2(a). Then let us imagine that as this curve C fully rotates about the axis $\mathbf{i}_z$ (without the bit advancing), the cutting profile surface (i.e., $\mathcal{S}$ or $\mathcal{S}'$ as illustrated in Fig. 2(b)) generated by the bit can be *equivalently replaced* by a rotation of the blade depicted in Fig. 2(a). Therefore, this curve describes the geometry of the *bit equivalent blade* and thus the bit shape.

In order to connect the concept of penetration per revolution and *equivalent blade*, we note that in the nominal case (steady drilling condition) the kinematic variable d_0 (produced per bit revolution in the time period $t_0 = 2\pi/\Omega_0$ with a nominal RPM Ω_0) is also the instantaneous depth-of-cut produced by the *equivalent blade*. Trivially, the rate of volume of rock excavated is equal to $\mathcal{Q}_0 = \Omega_0 d_0 \int_0^a r\mathrm{d}r = \frac{1}{2}a^2 d_0 \Omega_0$, and hence the total excavated rock volume rate per revolution is $\delta\mathcal{V}_0 = t_0 \mathcal{Q}_0 = \pi a^2 d_0$. If the interface laws are indeed rate-independent, the instantaneous depth-of-cut d associated with the rotation of the *bit equivalent blade* is the only kinematic variable needed. The laws account for the effect of bit shape (to represent all contributions of the orientations of PDC cutters on the bit).

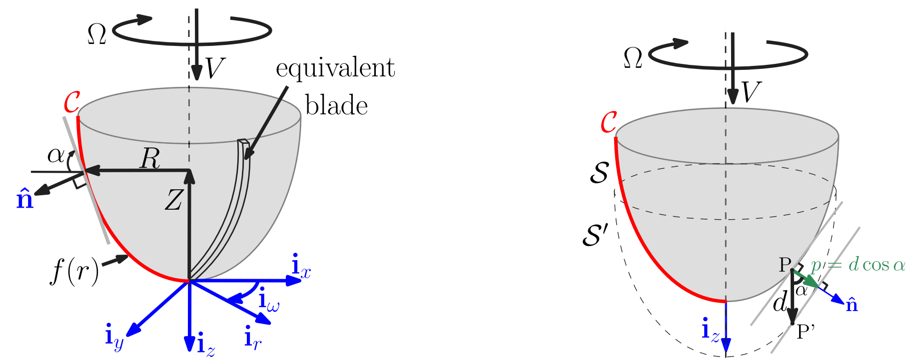

(a) An illustration of equivalent blade for a parabolic bit shape.

(b) The penetration (kinematic) variable d (after [25]).

Fig. 2. The PDC bit and its coordinate basis.

2.3. Bit profile

A PDC bit is characterized by its height b and its radius a. A radial coordinate R is the radial distance of a point located along the curve of the blade profile from the bit axis of symmetry (i.e., $0 \leq R \leq a$), while an axial coordinate Z is on the bit axis of symmetry with its origin at the lowest point on the bit (i.e., $0 \leq Z \leq b$); see Fig. 2(a). The function

$$z := f(r) \tag{2}$$

characterizes the bit profile (shape). This function maps the axial coordinate $z = {}^{Z}\!/_{a}$ on the radial coordinate $r = {}^{R}\!/_{a}$. In this work, we consider a parabolic bit shape function $f(r)$ as an illustrative example; see Fig. 2(a). However, these extended bit/rock interface laws are valid for a generic class of bit shapes, where we restrict the formulation of the interface laws to bit profiles with $f'(r) = {}^{\mathrm{d}f}\!/_{\mathrm{d}r} > 0$, for $0 \leq r \leq 1$. Note that if the bit has a re-entrant (nose) shape (for which $f(\cdot)$ is not invertible), the values of r can be multi-valued.

2.4. Local penetration

By reference to Fig. 2(b), let P be a point on the bit cutting profile $\mathcal{S}$, and P' the point on the cutting profile $\mathcal{S}'$ produced after the axial translation d by the rotation of the cutting edge curve $\mathcal{C}$. The local penetration variable p is then defined as the projection of vector $\overrightarrow{PP'}$ onto $\hat{\mathbf{n}}$, and equal to

$$p = d\cos\alpha, \tag{3}$$

where α is the angle between the external normal direction $\hat{\mathbf{n}}$ of the curve $\mathcal{C}$ and the direction $\mathbf{i}_z$ (see Fig. 2(a)), i.e., $\tan\alpha = {}^{\mathrm{d}f}\!/_{\mathrm{d}r}$. Hence we have

$$\cos\alpha = \frac{1}{\sqrt{(f'(r))^2 + 1}}. \tag{4}$$

The local penetration p varies along the cutting profile of the blade due to the effect of the bit shape (i.e., the profile function $f(r)$). Consequently, each elementary part of the *equivalent blade* only considers this local depth produced per revolution (in the view of local symmetry between the rotational axis of the bit $\mathbf{i}_z$ and the normal direction $\hat{\mathbf{n}}$ of the cutting profiles).

2.5. Bit engagement

We introduce an engagement parameter U that identifies the bit portion being engaged in the lower layer (as depicted in Fig. 3(b)) and acts as the evolution parameter for the weight and torque during the transitional phase. The dimensionless engagement parameter $u \in [0, {}^{b}\!/_{a}]$ is also introduced and is related to the parameter U scaled by the bit radius a:

$$u = \frac{U}{a}, \quad \text{for } 0 \leq U \leq b. \tag{5}$$

In its initial position, the bit is assumed to be fully engaged in the upper layer (i.e., $u = 0$) with its reference point located on the interface between the two layers. We also assume that the layer thickness $H \geq b$, which implies that the bit is at most engaging in these two consecutive layers during the transitional phase.

An alternative evolution parameter, $Q \in [0, a]$, is also considered. It is defined as the radial coordinate R of the point on the blade profile located at the interface, see Fig. 3(b). We consider its dimensionless form, $q = Q/a$, and use (2) to relate it with u in (5) according to

$$u = f(q), \quad \text{for } 0 \leq q \leq 1. \tag{6}$$

Parameter q is used to identify which part of the bit is engaged in the upper and lower rock layers, and can also be expressed uniquely in terms of u due to the invertibility of $f(\cdot)$ (due to its monotonicity): $q = f^{-1}(u)$, for $0 \leq u \leq {}^{b}\!/_{a}$.

2.6. Parameters of the cutter/rock interface laws

Previous works in Refs. 12, 13 have identified the cutter/rock properties that enter the interface laws when drilling *isotropic-homogeneous* rock formations (Fig. 3(a)). Firstly, the cutting component is parameterized by: *(i)* the intrinsic specific energy ε (in the unit of pressure), and *(ii)* the constant number ζ, characterizing the inclination of the cutting force. Secondly, the frictional contact component is parameterized by: *(i)* the coefficient of the friction μ (at the contact between the wear flat and rock), *(ii)* the maximum contact pressure σ at the wear flat interface, and *(iii)* the wear flat length ℓ that describes its state of wear (bluntness) of the cutter.

3. Bit/rock interface laws in the transitional phase

In this section, the interface laws in Refs. 12–14 will be extended to the transitional phase by relating the WOB and TOB to the depth-of-cut. Herein, we take into account the bit design properties, the state of wear (bluntness) of the bit, the mechanical properties of the rocks being drilled, and the evolution of the bit engagement in the two layers depicted in Fig. 3(b). In this extension, the upper and lower layers are characterized by their own distinct mechanical properties denoted by the subscripts u and l, respectively, i.e., ε_u, μ_u, σ_u for the upper layer and ε_l, μ_l, σ_l for the lower one.

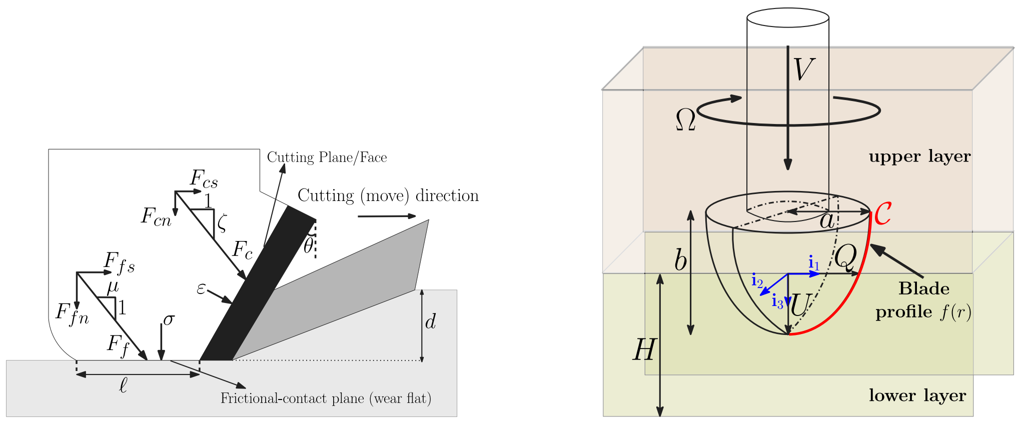

(a) A blunt single PDC cutter (after [12, 13]).	(b) The bit engagement.

Fig. 3. The PDC bit systems during the transitional phase.

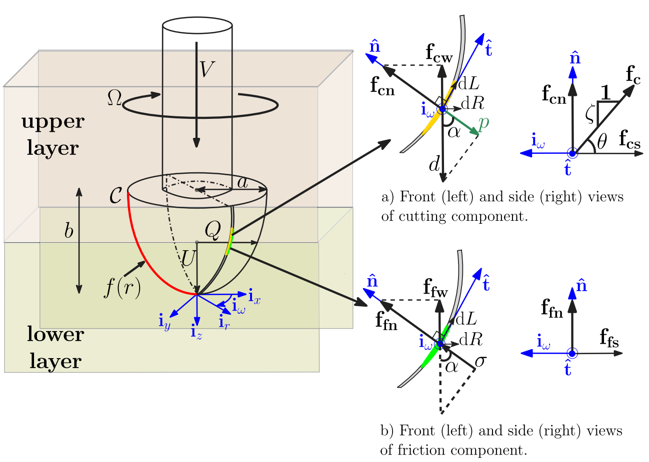

Fig. 4. Cutting and friction components of the weight-on-bit and torque-on-bit.

3.1. Cutting component

Consider the length L of the *equivalent blade* and its length element $\mathrm{d}L$ as depicted in Fig. 4 (the yellow-gold color; top-right). Note also that $\varkappa = L/a$ as the scaled length of the blade on the curvilinear coordinate s with respect to the bit profile (in dimensionless). The cutting force acting on this element $\mathrm{d}L$ is $\mathbf{f_c}\mathrm{d}L$, where $\mathbf{f_c}$ is the force density with dimension $[Force/Length]$. This force density can be decomposed into the horizontal component $\mathbf{f_{cs}}$ (along the surface) and the normal component $\mathbf{f_{cn}}$, i.e., $\mathbf{f_c} = -f_{cs}\mathbf{i}_\omega + f_{cn}\hat{\mathbf{n}}$; refer to the side view in Fig. 4. Herein, the torque on bit contributed by the cutting process is generated by the horizontal component, for which its magnitude f_{cs} is given by

$$f_{cs} = \varepsilon p. \tag{7}$$

Note that p is the local depth of penetration as described in (3). By considering the relation $\mathrm{d}R = \mathrm{d}L\cos\alpha$ (equivalently $\mathrm{d}r = \mathrm{d}s\cos\alpha$ in dimensionless), the torque (contributed by this horizontal force density) can be expressed by the following integration over the radial coordinate on the bit

$$T_c = a^2\int_0^{\varkappa} \varepsilon p r\,\mathrm{d}s = a^2\int_0^1 \varepsilon d\,r\,\mathrm{d}r = \frac{a^2}{2}\varepsilon d. \tag{8}$$

In the transitional phase, the integration process in (8) must take into account the bit engagement in the upper and lower layers, since the intrinsic specific energy ε differs for the two layers. Consequently, this integration is performed for adjusted intervals (i.e., for $r \in [0, q]$ for the lower layer and for $r \in [q, 1]$ for the upper layer), which yields

$$T_c = T_c^u + T_c^l = \frac{a^2}{2}d\left(\varepsilon_u\left(1-q^2\right) + \varepsilon_l q^2\right). \tag{9}$$

Next, for the cutting contribution to the weight-on-bit, we focus on the force density $\mathbf{f_{cn}}$ as depicted in the front and side views in Fig. 4. The vertical component of force density with magnitude $f_{cn}\cos\alpha$ can be integrated over the length element ds on the *equivalent blade* to yield the WOB due to the cutting process

$$W_c = a\int_0^{\varkappa} \zeta\varepsilon p\cos\alpha\,\mathrm{d}s = a\zeta d\int_0^1 \varepsilon\,\cos\alpha\,\mathrm{d}r = a\varepsilon d\zeta^*. \tag{10}$$

We define the nominal bit design parameter for the cutting component: $\zeta^* := \zeta\,\vartheta_\zeta$ with

$$\vartheta_\zeta := \int_0^1 \frac{1}{\sqrt{(f'(r))^2+1}}\mathrm{d}r, \tag{11}$$

as we recall (4) to explicitly combine the orientation of the local cutting force and the bit profile function $f(r)$ which both affect the WOB. As for the torque, the integral is split in two parts to account for the different properties of the two rock layers, which gives

$$W_c = W_c^u + W_c^l = ad\zeta\left(\varepsilon_u\int_q^1 \cos\alpha\mathrm{d}r + \varepsilon_l\int_0^q \cos\alpha\mathrm{d}r\right). \tag{12}$$

Similarly, from (4) and (12) we define the bit design parameters for both upper and lower layers ($\vartheta_\zeta^u(q)$ and $\vartheta_\zeta^l(q)$, respectively) as follows:

$$\vartheta_\zeta^u(q) := \frac{1}{\vartheta_\zeta}\int_q^1 \frac{1}{\sqrt{(f'(r))^2+1}}\mathrm{d}r, \qquad \vartheta_\zeta^l(q) := \frac{1}{\vartheta_\zeta}\int_0^q \frac{1}{\sqrt{(f'(r))^2+1}}\mathrm{d}r, \tag{13}$$

such that $\vartheta_\zeta^u(q)+\vartheta_\zeta^l(q) = 1$. By using (11) and (13) in combination with (4), W_c in (12) can be rewritten as

$$W_c = a\zeta^* d\left(\varepsilon_u\left(1-\vartheta_\zeta^l\right) + \varepsilon_l\,\vartheta_\zeta^l\right). \tag{14}$$

3.2. Frictional contact component

Consider an element of wear flat on the *equivalent blade* in Fig. 4 with the length element $\mathrm{d}L$ (e.g., the green color; bottom-right) for calculating the frictional components of the weight-on-bit and torque-on-bit. Due to the contact stress σ applied on the wear flat element in the normal direction $\hat{\mathbf{n}}$, the force density $\mathbf{f_{fn}}$ generates the weight-on-bit. This normal force density has magnitude

$$f_{fn} = \sigma\lambda. \tag{15}$$

In addition, the frictional force density $\mathbf{f_{fs}}$ in the horizontal direction (along the surface) generates to the torque-on-bit, and its has magnitude $f_{fs} = \mu f_{fn}$. Note that λ is the radial distribution of the wear flat length produced by each cutter on the blade. As we assume λ a uniform radial distribution of the wear flat length, the combined wear flat length on the contact surface of the *equivalent blade* is equal to ℓ in the horizontal direction of the blade (i.e., $\ell = \int_0^1 \lambda(r)\,\mathrm{d}r = \lambda$).

Herein, the weight acting on the bit due to the frictional contact is calculated along the blade length L using the curvilinear coordinate s with respect to the bit profile. By considering the scaled length $\varkappa = L/a$ and the relation $\mathrm{d}r = \mathrm{d}s\cos\alpha$, this frictional component of WOB can be written as the integral of the force density $f_{fw} = f_{fn}\cos\alpha$ with the radial coordinate r in the interval $r \in [0,1]$:

$$W_f = a\int_0^{\varkappa} \sigma\lambda\cos\alpha \mathrm{d}s = a\sigma\int_0^1 \lambda \mathrm{d}r = a\sigma\ell. \tag{16}$$

In the transitional phase, again the integration interval in (16) is adjusted using the coordinate q, and thus the associated rock parameters for the upper and lower layers are used. This leads to

$$W_f = W_f^u + W_f^l = a\,\ell\left(\sigma_u(1-q) + \sigma_l q\right). \tag{17}$$

Furthermore, the frictional force density with magnitude f_{fs} (using a Coulomb friction model) contributes to the torque that can be written in the following integral with the coordinate r in the same interval:

$$T_f = a^2\int_0^{\varkappa} \mu\sigma\lambda r\,\mathrm{d}s = a^2\mu\sigma\int_0^1 \frac{\lambda r}{\cos\alpha}\mathrm{d}r = \frac{a^2}{2}\mu\sigma\ell\xi, \tag{18}$$

as we consider a uniform radial distribution of the wear flat length ($\lambda = \ell$). We define the nominal bit parameter for the frictional contact (by recalling from (4) that $\sec\alpha = \sqrt{(f'(r))^2+1}$):

$$\xi := 2\int_0^1 r\sqrt{(f'(r))^2+1}\,\mathrm{d}r, \tag{19}$$

which is associated to the orientation of the contact force on the wear flat with respect to the bit shape $f(r)$.

In the transitional phase, we again adapt the interval of the integration in (18) for the torque with the coordinate q and use the associated rock parameters. This gives

$$T_f = T_f^u + T_f^l = a^2\ell\left(\mu_u\sigma_u\int_q^1 \frac{r}{\cos\alpha}\mathrm{d}r + \mu_l\sigma_l\int_0^q \frac{r}{\cos\alpha}\mathrm{d}r\right). \tag{20}$$

Similar to the cutting component, we also define the bit parameters of the frictional component for both upper and lower layers ($\vartheta_\xi^u(q)$ and $\vartheta_\xi^l(q)$, respectively) as follows:

$$\vartheta_\xi^u(q) := \frac{2}{\xi}\int_q^1 r\sqrt{(f'(r))^2+1}\,\mathrm{d}r, \qquad \vartheta_\xi^l(q) := \frac{2}{\xi}\int_0^q r\sqrt{(f'(r))^2+1}\,\mathrm{d}r, \tag{21}$$

such that $\vartheta_\xi^u(q) + \vartheta_\xi^l(q) = 1$ holds. Hence, by also considering the following relation obtained from (17):

$$a\,\ell = \frac{W_f}{\left(\sigma_u(1-q) + \sigma_l q\right)}, \tag{22}$$

the torque in (20) can be rewritten in terms of the weight W_f,

$$T_f = \frac{(\mu_u\sigma_u(1-\vartheta_\xi^l) + \mu_l\sigma_l\vartheta_\xi^l)\,a\,\xi}{2\left(\sigma_u(1-q) + \sigma_l q\right)}W_f. \tag{23}$$

Summarizing, Eqs. (9), (14), (17) and (23) represent the bit/rock interface laws, which map the depth-of-cut d to the weight-on-bit and torque-on-bit and also evolve with parameter q during the transitional phase.

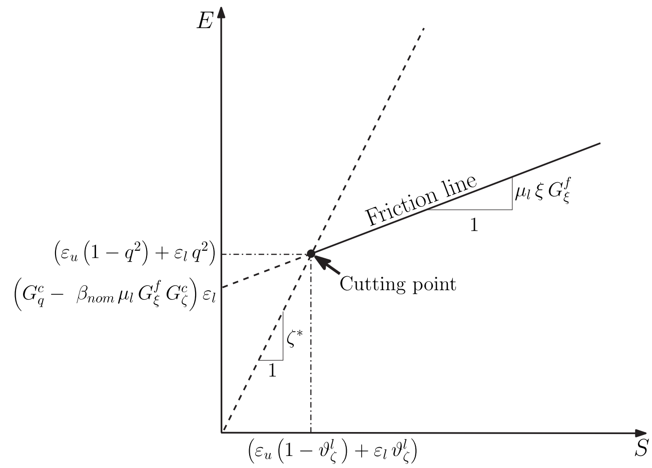

Fig. 5. $E-S$ diagram for a given value of the bit engagement parameter u under the variations of hook-load H_0 (determining the total weight-on-bit).

4. $E-S$ diagram and drilling efficiency in the transitional phase for *quasi-stationary* drilling

In this section, the bit/rock interface laws derived for the transitional case are used to extend the $E-S$ diagram and to derive expressions for the drilling efficiency. Under the assumed *quasi-stationary* drilling conditions, the weight-on-bit W applied by the BHA is in equilibrium with the reaction force resulting from the interaction of the cutters with the rock, i.e., $W = W_c + W_f$, where W_c and W_f are given in (14) and (17), respectively. Hence,

$$W = a\zeta\vartheta_\zeta\left(\varepsilon_u\left(1-\vartheta_\zeta^l\right) + \varepsilon_l\vartheta_\zeta^l\right)d + a\,l\left(\sigma_u(1-q) + \sigma_l q\right). \tag{24}$$

Solving (24) for the penetration variable d yields

$$d = \frac{\left(W - a\,l\left(\sigma_u(1-q) + \sigma_l q\right)\right)}{a\zeta\vartheta_\zeta\left(\varepsilon_u\left(1-\vartheta_\zeta^l\right) + \varepsilon_l\vartheta_\zeta^l\right)}. \tag{25}$$

Here, we see that the kinematic variable d is a continuous function of the engagement u via the parameter q according to (6).

4.1. $E-S$ diagram for the transitional phase

Mechanical-specific-energy (MSE) E is the quantity (in the unit of pressure) representing the amount of energy dissipated to drill a unit volume of rock. It accounts for both the work spent to fragment (cut) the rock and for frictional dissipation, and is defined as follows:

$$E := \frac{2T}{a^2 d}, \tag{26}$$

with the total TOB $T = T_c + T_f$, where T_c and T_f are given in (9) and (23), respectively. Drilling strength S is defined as the quantity (in the unit of pressure) that reflects the axial force imposed on the PDC bit for producing the penetration variable d:

$$S := \frac{W}{ad}. \tag{27}$$

By noting the relation between the torque T_f and the weight W_f in (23), the definition of MSE E in (26) can be rewritten in terms of drilling strength S with respect to the bit engagement u (or equivalently $q = f^{-1}(u)$) as follows:

$$E = \left(G_q^c - \beta_{nom}\mu_l G_\xi^f G_\zeta^c\right)\varepsilon_l + \mu_l\,\xi\,G_\xi^f\,S, \tag{28}$$

with the following definitions:

$$G_q^c := \left(g_\varepsilon\left(1-q^2\right) + q^2\right), \qquad G_\xi^f := \frac{(g_\mu g_\sigma(1-\vartheta_\xi^l) + \vartheta_\xi^l)}{(g_\sigma(1-q) + q)},$$

$$G^c_\zeta := \left(g_\varepsilon\left(1-\vartheta^l_\zeta\right)+\vartheta^l_\zeta\right), \qquad \beta_{nom} := \xi\,\zeta^*. \tag{29}$$

Here, we define the ratio of the associated rock mechanical parameters in the cutting and frictional contact components of the interface laws for two distinct rock layers as follows:

$$g_\varepsilon := \frac{\varepsilon_u}{\varepsilon_l}, \qquad g_\mu := \frac{\mu_u}{\mu_l}, \qquad g_\sigma := \frac{\sigma_u}{\sigma_l}. \tag{30}$$

This analytical expression of MSE characterizes the friction line illustrated in Fig. 5 for a particular value of parameter u; this is what we call the 2D $E-S$ diagram. Visualizing the dependency of E and S on u will lead to a 3D $E-S$ diagram, and an example will be presented in Section 5.

4.1.1. Cutting point

An ideally sharp bit blade (characterized by a wear flat length $\ell \approx 0$) is represented by the so-called cutting point in the $E-S$ diagram (the left-most point on the friction line in Fig. 5). At the cutting point, all the energy received by the bit is entirely used for the cutting process without any frictional dissipation ($W_f = T_f = 0$). For $W_f = 0$, the nominal value of depth-of-cut in (25) at the cutting point becomes

$$d_{cp} = \frac{W}{a\,\zeta\,\vartheta_\zeta\left(\varepsilon_u\left(1-\vartheta^l_\zeta\right)+\varepsilon_l\,\vartheta^l_\zeta\right)}. \tag{31}$$

For the cutting point, the MSE E and drilling strength S can be expressed as

$$E_{cp} = \frac{2T_c}{a^2 d_{cp}} = \left(\varepsilon_u\left(1-q^2\right)+\varepsilon_l\,q^2\right), \tag{32}$$

$$S_{cp} = \frac{W_c}{a d_{cp}} = \zeta^*\left(\varepsilon_u\left(1-\vartheta^l_\zeta\right)+\varepsilon_l\,\vartheta^l_\zeta\right), \tag{33}$$

with the nominal bit parameter of the cutting component $\zeta^* = \zeta\,\vartheta_\zeta$; see in (11). This cutting point is also explicitly depicted in Fig. 5 and depends on the parameter u.

4.2. Drilling efficiency

The drilling efficiency is defined as the ratio between the intrinsic specific energy of the associated rock layer and the *apparent* specific energy,[12,13] represented by the MSE E. Thus for the transitional phase considered here, we refer to (32) for the intrinsic specific energy of the two rock layers and (28) for the MSE E. Hence, the drilling efficiency during the transitional phase is given by

$$\eta(q) = \frac{E_{cp}}{E} = \frac{\left(\varepsilon_u\left(1-q^2\right)+\varepsilon_l q^2\right)}{\left(G^c_q - \beta_{nom}\,\mu_l\,G^f_\xi\,G^c_\zeta\right)\varepsilon_l + \mu_l\,\xi\,G^f_\xi\,S}. \tag{34}$$

The drilling efficiency evolves during the transitional phase in view of the dependence of q on the engagement u.

5. Illustrative case study and analysis

Next, we illustrate the $E-S$ diagram and the drilling efficiency during the transition of the bit between two rock layers.

5.1. $E-S$ diagram for the transitional phase: a transition from soft to hard layers

During the transitional phase, E and S depend on the bit engagement parameter $u \in [0, b/a]$. For the illustrative case study presented below, we consider the rock mechanical properties and the physical characteristics of the drag bit listed in Table 1. A parabolic bit is considered, with $f(r) = A_z r^2$, where A_z is a positive constant.

Fig. 6 illustrates the evolution of MSE E in terms of drilling strength S as the bit transitions from a soft to a hard layers. Specifically, this 3D E–S diagram is depicted as a *friction surface* that maps all possible 2D *friction lines* for each bit engagement progression u into the lower layer (i.e., the dashed lines for fixed values of u). As such, this 3-D E–S diagram constrains all the possible states of the bit response irrespective of the WOB and the wear state of the bit.

Table 1
Bit and rock mechanical properties for soft and hard layers.

Parameter name	Soft layer	Hard layer	Unit
Intrinsic specific energy (ε)	100	200	MPa
Contact pressure (σ)	100	200	MPa
Friction coefficient (μ)	0.5	1.0	[–]
Bit height (b)	22.2	22.2	cm
Bit radius (a)	10.8	10.8	cm

For this particular example, the friction lines for several selected bit engagement u values are depicted in dashed-gray lines. The solid lines characterize the transition from the soft-upper layer ($u = 0$ in green-square) to the hard-lower layer ($u = b/a$ in blue-square) for a constant weight W applied to the PDC bit. The green and blue squares represent the 2D friction lines for the homogeneous cases when the bit is fully engaged in the soft and hard rock layers, respectively. Increasing the weight W moves the solid lines close to the red *cutting line* (reflecting the ideal - no dissipation condition). The cutting points also evolve during the transition as a *cutting line* indicated by the red solid line and only dependent on the bit/rock parameters — conforming (32) for E_{cp} and (33) for S_{cp}.

Fig. 7(a) shows the 2D projections of the 3D E–S diagram (in Fig. 6) based on several selected values of u. The dashed lines show the friction lines for each u; see also the analytical sketch in Fig. 5. In addition, Fig. 7(b) shows the 2D projection (in solid gray lines) of the 3D $E-S$ diagram for each constant level of the applied weight W, when the bit traverses the interface from the soft-upper layer to the hard-lower one. An important observation on the basis of Figs. 6 and 7(b) is that the bit is constrained to *nonlinear* curves in $E-S$ space during the transition at a constant weight-on-bit.

5.2. Drilling efficiency in transitional phase

Now we illustrate the variation of drilling efficiency given by (34) in a *soft-to-hard* layers transition. As shown in Fig. 8(a), the drilling efficiency increases with the increasing applied weight W, and these efficiency lines move closer to an efficiency $\eta = 1$ (the red cutting line) in which no frictional contact dissipation occurs. As expected, in a *soft-to-hard* layers transition the drilling efficiency decreases with the progression of u, and this confirms the reduction in the depth-of-cut d.

5.2.1. Comparison of the drilling efficiency for different bit profiles within the transition from soft to hard layers

Notably, the transition of the drilling efficiency shows a nonlinear dependency on u, which is related to the bit shape embodied in the function $f(r)$. To assess the effect of bit profile on the drilling efficiency, we compare two different ideal bit profiles: *(i)* a linear function $f(r) = A_z r$, *(ii)* a parabolic function $f(r) = A_z r^2$), both for a *soft-to-hard* layers transition.

Fig. 8(b) reveals that the drilling efficiency for the parabolic profile shows more drop-off in the early phase of the transition (i.e., for small values of the engagement u) as compared to the drilling efficiency of the linear profile. This can also be understood by realizing that, for small values of u for the parabolic bit shape, a larger (radial) portion of the bit is engaged within the lower (hard) layer than for the same value of u for the linear bit profile — see in the inset in Fig. 8(b). This inset shows both the linear and parabolic bit profiles with the same height and radius of which the values are listed in Table 1. Consequently, these give different values of the coordinate q and the bit parameters ϑ^l_ζ and ϑ^l_ξ for the cutting and frictional components, respectively, (see (29)) for the calculations of drilling efficiency in (34).

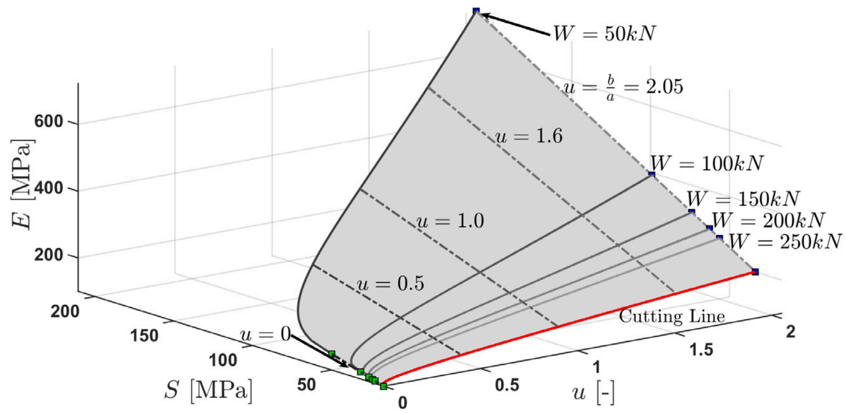

Fig. 6. 3D $E-S$ diagram under the variations of weight W applied at the top side of PDC bit during the transitional phase from a soft-upper layer (green-square) to a hard-lower layer (blue-square). (For interpretation of the references to color in this figure legend, the reader is referred to the web version of this article.)

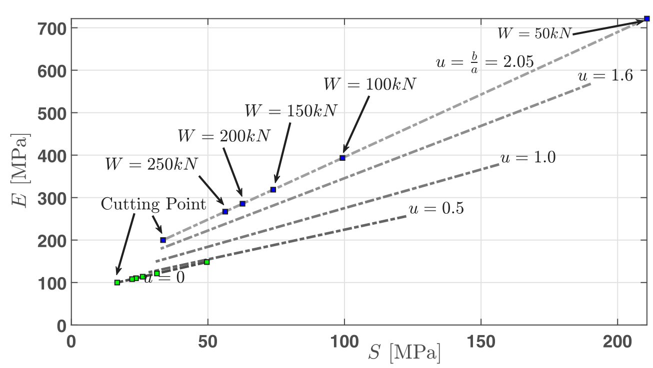

(a) 2D projection for the selected values of u.

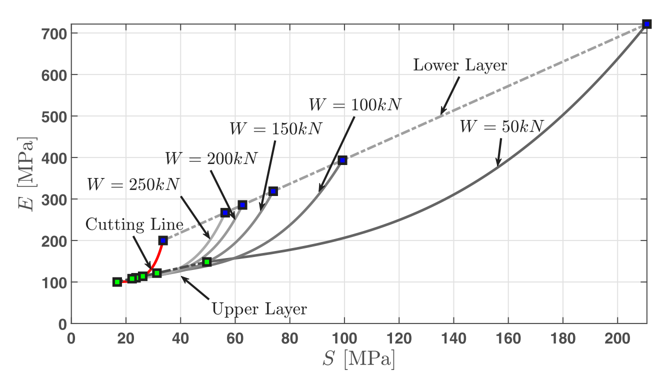

(b) 2D projection based on the variations of W.

Fig. 7. 2D projections of 3D $E-S$ diagram for the transitional phase of bit motion from the soft-upper layer (green-square) to the hard-lower layer (blue-square). (For interpretation of the references to color in this figure legend, the reader is referred to the web version of this article.)

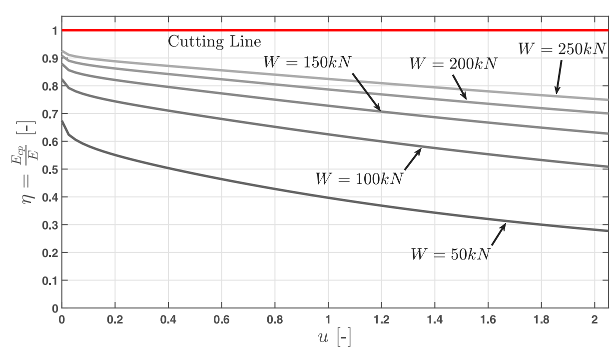

(a) Drilling efficiency with the variations of applied weight W.

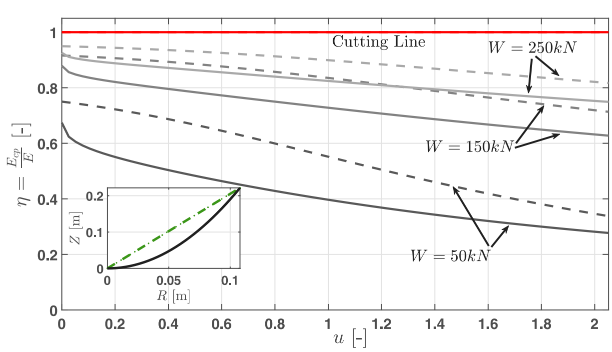

(b) Drilling efficiencies comparison for both linear (dashed line) and parabolic (solid line) bit profiles.

Fig. 8. Drilling efficiency during the transitional phase of bit motion from a soft-upper layer to a hard-lower layer ($u = 0$: fully in soft layer, $u = b/a = 2.05$: fully in hard layer). The dashed line is for the linear profile, while the solid line is for the parabolic profile.

6. Conclusions

This study has extended the bit/rock interface laws of fixed cutter (PDC) bits, developed earlier in Refs. 12–14 for homogeneous formations, to the case of a bit transitioning between two different rock layers. In particular, the extended formulation of the interface laws involves the adaptation of the rock mechanical properties and bit-design parameters used in the cutting and frictional contact components of the laws. Based on this novel bit/rock interaction model we, firstly, constructed 3D $E-S$ diagrams and, secondly, analyze the drilling efficiency as a function of the bit engagement in the transitional phase between two layers. From the numerical examples, these aspects have shown distinct characteristics of dynamic and kinematic variables between the homogeneous formation and two-layered formation. In addition, it has been shown that the 3D $E-S$ diagram and the drilling efficiency are highly dependent on the bit shape for such transitional phase (via the bit engagement) and deviate essentially from the well-known 2D $E-S$ diagram for homogeneous formation. This shows the relevance of these novel bit/rock interface laws for analyzing drilling efficiency. In addition, these interface laws can also be used in the scope of dynamic drill–string models for layered formations (e.g., for the analysis of vibrations).

Declaration of competing interest

The authors declare that they have no known competing financial interests or personal relationships that could have appeared to influence the work reported in this paper.

Acknowledgment

This study is supported by the Indonesian Endowment Fund for Education (LPDP) of the Republic of Indonesia (Grant No. PRJ-4653/LPDP.3/2016).

References

1. Smith bits - A Schlumberger Company. Product catalog. 2018.
2. Zamudio CA, Tlusty JL, Dareing DW. Self-excited vibrations in drillstrings. In: 62nd Annual Technical Conference and Exhibition of SPE. 1987:117–124.
3. Dareing D, Tlusty J, Zamudio C. Self-excited vibrations induced by drag bits. *J Energy Resour Technol*. 1990;112:54–61.
4. Gerbaud L, Men S, Sellami H. PDC bits: all comes from the cutter rock interaction. In: IADC/SPE Drilling Conference, number IADC/SPE-98988. 2006.
5. Hyne NJ. *Nontechnical Guide to Petroleum Geology, Exploration, Drilling and Production*. 3rd ed. PennWell Corporation; 2012.
6. Beeh HA, Khalil H, Paulus SL, Tiku A, Karlsen BA. Thorough analysis and commitment for improvement led to a step change in the drilling performance on Valemon field, North Sea. In: SPE Norway One Day Seminar. 2018.
7. Dupriest FE, Noynaert S, Cunningham T, Rendon M. Maximizing drilling performance through the Delaware Basin Brushy Canyon and interbedded formations. In: IADC/SPE Drilling Conference, number IADC/SPE-199599-MS. 2020.
8. Mensa-Wilmot G, Fear MJ. The effects of formation hardness, abrasiveness, heterogeneity and hole size on PDC bit performance. In 2001 SPE/IADC Drilling Conference, number SPE/IADC-67698, 2001.
9. Brown ET, Green SJ, Sinha KP. The influence of rock anisotropy on hole deviation in rotary drilling - a review. *Int J Rock Mech Min Sci Geomech Abstracts*. 1981;18(5):387–401.
10. Boualleg R, Sellami H, Men S. Effect of formations anisotropy on directional tendencies of drilling systems. In: 2006 SPE/IADC Drilling Conference, number SPE/IADC-98865, 2006.
11. Aird P. *Deepwater Drilling: Well Planning, Design, Engineering, Operations, and Technology Applications*. Elsevier Ltd.; 2019.
12. Detournay E, Defourny P. A phenomenological model for the drilling action of drag bits. *Int J Rock Mech Min Sci Geomech Abstracts*. 1992;29(1):13–23.
13. Detournay E, Richard T, Shepherd M. Drilling response of drag bits: theory and experiment. *Int J Rock Mech Min Sci*. 2008;45(8):1347–1360.
14. Zhou Y, Detournay E. Analysis of the contact forces on a blunt PDC bit. In: *48th US Rock Mechanics / Geomechanics Symposium 2014*. American Rock Mechanics Association (ARMA); 2014:306–314. vol. 1.
15. Richard T, Germay C, Detournay E. A simplified model to explore the root cause of stick–slip vibrations in drilling systems with drag bits. *J Sound Vib*. 2007;305:432–456.
16. Germay C, Wouw Nvande, Nijmeijer H, Sepulchre R. Nonlinear drillstring dynamics analysis. *SIAM J Appl Dyn Syst*. 2009;8(2):527–553.
17. Besselink B, Wouw Nvande, Nijmeijer H. A semi-analytical study of stick–slip oscillations in drilling systems. *J Comput Nonlinear Dyn*. 2011;6:21006–21009.
18. Depouhon A, Detournay E. Instability regimes and self-excited vibrations in deep drilling systems. *J Sound Vib*. 2014;333(7):2019–2039.
19. Liu X, Vlajic N, Long X, Meng G, Balachandran B. Coupled axial-torsional dynamics in rotary drilling with state-dependent delay: stability and control. *Nonlinear Dynam*. 2014;78(3):1891–1906.
20. Insperger T, Stépán G, Turi J. State-dependent delay in regenerative turning processes. *Nonlinear Dynam*. 2007;47(1–3):275–283.
21. Deliac EP. *Optimisation Des Machines D'Abattages à Pics* [Ph.D. thesis]. Université Pierre et Marie Curie; 1986.
22. Nishimatsu Y. Theories of rock cutting. In: Hudson JA, ed. *Comprehensive Rock Engineering: Principles, Practice, and Project*. 1993:647–662. vol. 1, [chapter 26].
23. Franca LFP. Drilling action of roller-cone bits: Modeling and experimental validation. *ASME J Energy Resour Technol*. 2010;132(4). 043101–1 043101–9.
24. Richard T, Dagrain F, Poyol E, Detournay E. Rock strength determination from scratch tests. *Eng Geol*. 2012;147–148:91–100.
25. Perneder L, Detournay E, Downton G. Bit-rock interface laws in directional drilling. *Int J Rock Mech Min Sci*. 2012;51:81–90.